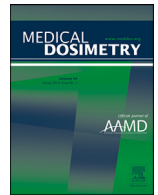




ELSEVIER

Medical Dosimetry

journal homepage: www.meddos.org

Dosimetry Contribution

Novel hybrid treatment planning approach for irradiation a pediatric craniospinal axis

Dr. Christian Ziemann^{†,*}, Florian Cremers[†], Laura Motisi[‡], Dirk Albers[§], Miller MacPherson[#], Dirk Rades[†]

[†] Department of Radiotherapy, University Medical Center Schleswig Holstein/Campus Luebeck, Luebeck, Germany

[‡] Department of Radiation Oncology, University Hospital Zürich, Zürich, Suisse

[§] Department of Radiotherapy and Radiation Oncology, University Medical Center Hamburg-Eppendorf, Hamburg, Germany

[#] University of Ottawa, The Ottawa Hospital, Department of Radiology, Radiation Oncology, and Medical Physics, Ottawa, Canada

ARTICLE INFO

Article history:

Received 22 March 2023

Revised 19 July 2023

Accepted 26 August 2023

Available online xxx

Keywords:

Medulloblastoma

Craniospinal axis irradiation

Hybrid treatment

ABSTRACT

This study presents a new treatment planning approach merging 3D-CRT and VMAT fields into a hybrid treatment plan (HybTP), in order to achieve an optimum dose coverage of the planning target volume (PTV) and protection of OAR. Craniospinal axis irradiation (CSI) treated with 3D conformal radiotherapy (3D-CRT) is associated with high doses to the heart and eye lenses but provides better sparing of lungs and kidneys compared to volumetric modulated arc therapy (VMAT). VMAT treatment spares eye lenses and the heart, but lungs and kidneys are not as effective as 3D-CRT. Thus, a combination of both techniques (HybTP) may be optimal in sparing all these organs at risk (OAR). The results of HybTP are compared with helical tomotherapy (HT), intensity modulated radio therapy (IMRT), VMAT, and 3D-CRT plans. Hybrid, HT, VMAT, IMRT, and 3D-CRT treatment plans for a male child (age 6 years) with medulloblastoma were created and compared. A total dose of 35.2 Gy (PTV) with a dose per fraction of 1.6 Gy was prescribed. The following dose acceptance criteria were defined:

- (1) Mean PTV dose should be 100% of the prescribed dose, while the maximum dose should not exceed 107%.
- (2) At least 98% of the PTV should receive 95% of the prescribed dose.
- (3) The cribriform plate should be covered by the 95% isodose line.
- (4) The acceptance criteria for the OARs were: lenses $D_{max} < 10$ Gy, lungs $D_{mean} < 7$ Gy, kidneys $D_{mean} < 15$ Gy, heart $D_{mean} < 26$ Gy, and heart $V_{25} < 10\%$.

The plans were compared regarding dose homogeneity index (HI) and conformity index (CI), PTV coverage, (particularly at cribriform plate) and doses at OARs. Best conformity was achieved with HT (CI = 0.98) followed by VMAT (CI = 0.96), IMRT (CI = 0.91), HybTP (CI = 0.86), and 3D-CRT (CI = 0.83). The homogeneity index varied marginally. For both HT and IMRT the HI was 0.07, and for 3D-CRT, VMAT and HybTP the HI was between 0.13 and 0.15. The cribriform plate was sufficiently covered by HybTP, VMAT, and 3D-CRT. The dose acceptance criteria for OARs were met by HT and HybTP. VMAT did not meet the criteria for lung ($D_{mean} = \text{right } 10.4 \text{ Gy/left } 10.2 \text{ Gy}$), 3D-CRT did not meet the criteria for eye lenses ($D_{max} = \text{right } 32.3 \text{ Gy/left } 33.1$), and heart ($V_{25} \approx 44\%$) and IMRT did not meet the criteria for lung ($D_{mean} = \text{right } 11.1 \text{ Gy/left } 11.2 \text{ Gy}$) and eye lenses ($D_{max} = \text{right } 12.2 \text{ Gy/left } 13.1$). HybTP meets all defined acceptance criteria and has proved to be a reasonable alternative for CSI. With HybTP that combines VMAT at the brain and heart with 3D-CRT posterior spinal fields (to spare lungs and kidneys), both appropriate coverage of the PTV and sparing of OAR can be achieved.

© 2023 The Authors. Published by Elsevier Inc. on behalf of American Association of Medical Dosimetrists.

This is an open access article under the CC BY-NC-ND license (<http://creativecommons.org/licenses/by-nc-nd/4.0/>)

* Reprint request to Dr. Christian Ziemann, Department of Radiotherapy, University Medical Centre Schleswig Holstein/Campus Luebeck, Ratzeburger Allee 160, 23538 Luebeck, Germany.

E-mail address: christian.ziemann@uksh.de (C. Ziemann).

<https://doi.org/10.1016/j.meddos.2023.08.011>

0958-3947/© 2023 The Authors. Published by Elsevier Inc. on behalf of American Association of Medical Dosimetrists. This is an open access article under the CC BY-NC-ND license (<http://creativecommons.org/licenses/by-nc-nd/4.0/>)

Introduction

Medulloblastoma is the most common malignant embryonal tumor of the central nervous system (CNS) in children and accounts for nearly 20% of all brain tumors in this age group. Surgical resection followed by radiation- and chemotherapy is the commonly used treatment.¹⁻⁸ Five-year survival rates range between 20% and 100%, depending on age, metastatic spread, and subtypes of medulloblastoma.^{9,10} When performing radiotherapy, the entire craniospinal axis (CSA) has to be irradiated to reduce the risk of dissemination of primary CNS tumors through cerebrospinal fluid flow (CSF) pathways and improve survival.^{11,12,39} During treatment planning particular consideration must be given to the cribriform plate. The risk for patients to develop a recurrence in this structure is about 15% if it is not appropriately treated.^{3,13-17,54}

Patients receiving radiation therapy may experience long-term side effects such as neuroendocrine dysfunction, hearing disability, cataract formation,⁴⁵ cognitive deficits, and cardiac sequelae, along with impaired growth and the risk of developing radiation-induced secondary malignancies.¹⁸⁻²³ To reduce these side effects, craniospinal axis irradiation (CSI) must consider a variety of organs at risk (OAR) additionally to the complex planning target volume (PTV). This makes treatment planning for CSI a challenging and complex process. The use of multiple isocenters and the alignment of a large number of fields to obtain satisfactory plans further add to this challenge.^{4,22,24,25}

Three-dimensional conformal radiotherapy (3D-CRT) with static fields represents a commonly used conventional radiation technique for CSI. Two bilateral half-beam blocked cerebral fields are collimated to match the divergence of an adjacent inferior spinal field.^{7,18,25-28} The spinal field makes the 3D-CRT suitable for dose sparing of lungs and kidneys. However, the exit dose of this field passes directly through the heart resulting in a high cardiotoxicity.^{25,29,56} If the cribriform plate is part of the cerebral PTV, the dose savings of the ocular lenses cannot be realized. Both organs get into an overlapping position and shielding the lenses by the multileaf collimator (MLC) is then no longer possible.^{30,49,54} In general, 3D-CRT is quite limited with regard to highly individualized treatment plans customized to specific patient needs, for example, dose sparing of the hippocampus or hypothalamus.³¹

Intensity modulated radiotherapy (IMRT) and volumetric modulated arc therapy (VMAT) offer promising approaches in the treatment of CSA.^{4,24,25,27,28,32-34,52-55} Even with consideration of the cribriform plate as part of the PTV, a significant dose reduction to the eye lenses can be realized. However, IMRT and VMAT are often not able to match dose sparing for the lung and kidneys that is achievable with the spinal field configuration of the 3D-CRT method. Furthermore, it results in a larger irradiated volume of normal tissue that should be considered when treating young patients.²⁵ Goitein et al. pointed out that the volume receiving low doses should be minimized to avoid radiation-induced secondary tumors in this region as a long-term side effect.³⁵

Helical tomotherapy (HT) offers the possibility of irradiating large volumes continuously.^{4,28,36-38} It ensures irradiation of the entire CSA in one session without field junctions. An elective dose reduction to all OARs and the verification of patient position via computed tomography (CT) prior to irradiation is possible. The conformity indices (CI) and homogeneity indices (HI) resulting from the dose distribution are better than those achievable with 3D-CRT. However, with HT a relatively large low-dose irradiation volume is created and hence a higher risk of inducing secondary neoplasias or giving rise to concerns about pulmonary toxicity caused by the treatment.^{38,37,41-43,51} But the arguments for treating medulloblastoma with HT in terms of PTV dose coverage

and sparing OARs are convincing. Although in the majority of radiotherapy centers expensive HT technology is not available, dose values achievable with HT can serve as a benchmark for CSI at conventional LINACS.

As described above, with forward-planned 3D-CRT and the inverse-planned IMRT and VMAT techniques 2 fundamentally different concepts exist for irradiating CSA using a conventional LINAC.⁴⁴ 3D-CRT leads to better sparing of lungs and kidneys compared to VMAT, whereas VMAT is more effective in sparing eye lenses. If it were possible to merge the 2 concepts into a hybrid that combines the advantages of both techniques and reduces the disadvantages, a third concept would emerge that ambitiously attempts to meet the HT benchmark as closely as possible. This would be an additional CSI planning option for radiotherapy facilities not equipped with HT. The technical challenge consists of matching inverse planned modulated fields to adjacent forward planned 3D-CRT fields. The resulting dose distribution must be homogeneous at the field junctions and along a large PTV with multiple isocenters. Toxicities for lungs and kidneys should be in the range of 3D-CRT, and the dose at the lenses and the dose to the heart comparable with values of modulated techniques. Dose conformity and homogeneity should be at least equal or better than that of 3D-CRT. To achieve these goals a novel Hybrid Treatment Planning (HybTP) technique was developed.

Methods and Materials

A male 6-year-old child with a medulloblastoma was positioned in head-first supine orientation which provides free access for anesthesia, immobilized in a vacuum mattress (Unger Medizintechnik, Muehlheim-Kaerlich, Germany) from the shoulder to the feet. An individual adapted thermoplastic mask (Unger Medizintechnik, Muehlheim-Kaerlich, Germany) was used to fix the head against movement.

CT acquisition (40-slice Biograph mCT, Siemens AG, Erlangen, Germany) of the whole body from cranium until the lesser trochanter (1mm slice) without contrast medium was done. The CT was transferred to ARIA[®] oncology information system (Version 15.1, Varian Medical Systems, Palo Alto, CA) where it was further processed for delineation and dose calculation in the treatment planning system (TPS) Eclipse[™] (Version 15.1, Varian Medical Systems, Palo Alto, CA).

Imaging studies (pre- and postoperative MRI of the brain and the spinal cord with and without contrast medium) were used to delineate target volumes and a fusion of the MRI and CT was performed.

All volumes were delineated as recommended in the international delineation guideline of target volumes.³⁹ The whole brain clinical target volume (CTV) including the whole brain with the cribriform plate region, the pituitary fossa, up to the inferior margin of the temporal lobes, and excluding the petrous bone and the basicranium. The whole spine CTV covered the entire spinal canal and the thecal sac, including the subarachnoid space, the intervertebral foramina, and the first cervical nerve roots. The final PTV was created by the CTV+3 mm margins.

3D-CRT-, IMRT- and VMAT treatment planes were created for a CLINAC 2100 DHX (Varian Medical Systems, Palo Alto, CA), equipped with a Millenium 120 MLC. All plans were calculated with 6MV photon beams to avoid neutron contamination, the dose rate was set to 600 MU/min. The plans contained 3 isocenters (IC), the IC were adjusted by longitudinal patient-couch movements. The source to axis distance (SAD) was kept constant.

For all plans a total dose of 35.2 Gy with a single dose of 1.6 Gy per fraction was prescribed.

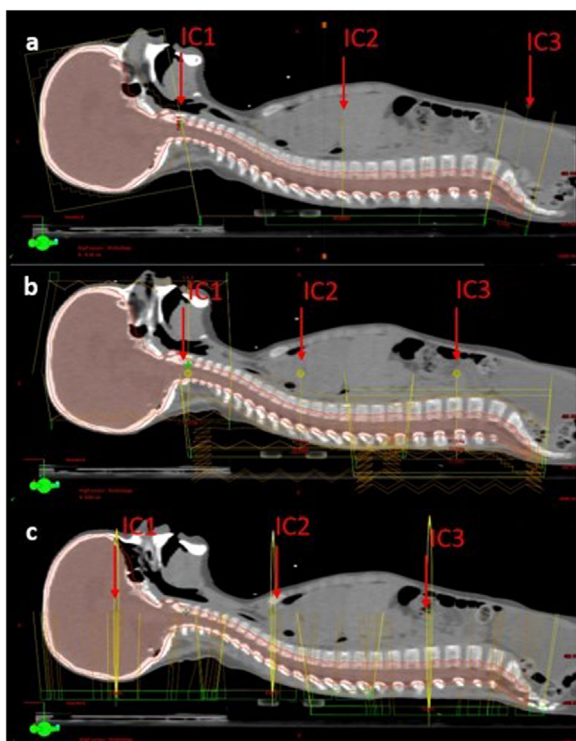


Fig. 1. Field setups with IC1-IC3, (A) 3D-CRT, (B), IMRT, (C) VMAT. (Color version of figure is available online.)

3D conformal radiation therapy (3D-CRT)

A treatment plan was generated (Fig. 1A) containing 2 opposing lateral fields at the brain (IC1), half beam blocked to match a supine field along the spine PTV at 180° Gantry angle (IC2). A lower spine field was matched by 90° patient couch rotation and an appropriate gantry angle (IC3). The MLCs were fitted to the PTV with a margin of 0.5 cm to spare the OARs without compromising the PTV. For dose homogenization the field-in-field function of the TPS was used. A field setup overview of 3D-CRT is shown in Fig. 1A.

Intensity modulated radiotherapy (IMRT)

The IMRT planning contains 12 brain fields at IC1 with a regular angular shift of 30° beginning from 0°. In supine position there are 3 fields at IC2 and additional 3 fields at IC3 with gantry angles of 120°, 180°, and 240°. In longitudinal direction the fields were generated with an overlap of 10 cm to achieve a homogenous dose distribution along the field junctions. Dose reduction in the OAR and PTV dose coverage has been performed in the optimization module of the TPS. After completing the optimization process, the fluence editing tool was used in order to remove hot and cold spots. Figure 1B shows a field setup overview of IMRT.

Volumetric modulated arc therapy (VMAT)

In Fig. 1C the VMAT field configuration with three 360° rotations is shown. At the brain 3 VMAT fields were applied at IC1; 2 main fields enclosed the brain PTV completely (collimator: 30° and 330°), and a third support field (collimator 90°) was restricted to the height of the orbital by reducing Y-blade to 6.7 cm. This third field was used to optimize the dose coverage at the cribriform plate while protecting the eye lenses by MLCs moving between the eyes perpendicular to the Y-blade. In the lung region two

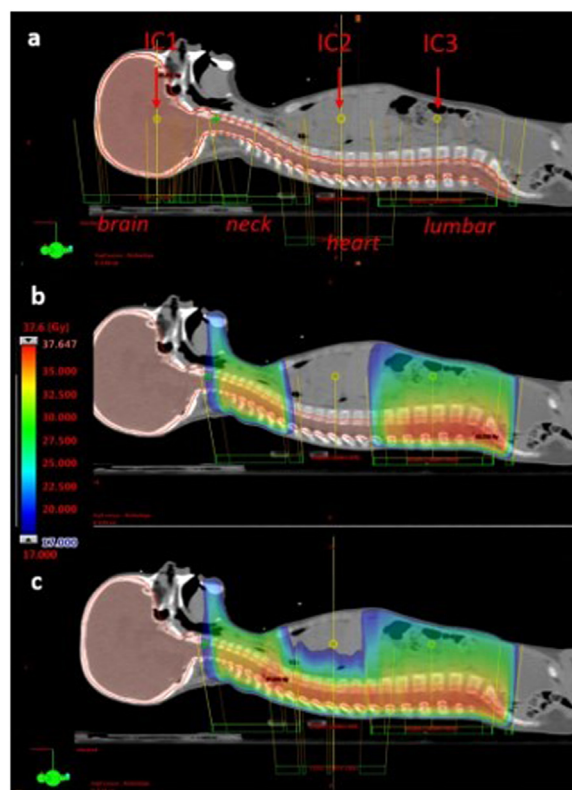


Fig. 2. (A) Field configuration HybTP (IC1-IC3), PTV in red, (B) calculated sub sections neck and lumbar, (C) complete calculated spine section (neck, heart, lumbar). Dose is shown in color wash, scaled from 17 to 37.6 Gy (± 48 -107%). (Color version of figure is available online.)

VMAT fields (IC2) and 2 VMAT fields in the lumbar region (IC3) completed the technique (collimator at both IC: 10° and 350°). To achieve a homogenous dose distribution along the field junctions, the fields were planned with an overlap of 10 cm.

The sparing of the OAR (lungs, kidneys and heart) was achieved by successive adaptation of the planning objectives in the TPS until the doses in the OAR have been reduced to minimum values as long as the dose sufficiently covers the PTV. The field setup overview of VMAT is shown in Fig. 1C below.

Hybrid treatment planning (HybTP)

When planning the HybTP the PTV is divided into two sections: brain PTV (IC1) and spine PTV (IC2 and IC3). The spine PTV is subdivided into 3 subsections: neck (IC2), heart (IC2) and lumbar (IC3) subsections (Fig. 2A). The planning starts in a first step with generating the neck and lumbar subsections as 3D-CRT supine fields shown in Fig. 2B. The 3D-CRT neck subsection is part of the HybTP lung sparing strategy. The field covers the spine PTV from approx. 1 cm inferior the skull base until the aortic arch. About one third of the field extends into the lung volume thus that can be shielded by the MLC. The lumbar 3D-CRT subsection field covers the spine PTV from 1.5 cm inferior the heart to 1.5 cm caudal the spine PTV and minimizes the irradiated volume of the kidneys. For both fields the MLCs were fitted to the PTV with a margin of 0.5 cm. In a second step a single VMAT arc was generated for closing the gap between the neck and lumbar 3D-CRT fields (heart subsection, Fig. 2C). Dose control of heart and lungs as well as the spine PTV dose coverage was performed by using the VMAT optimization module, the dose base plan function was used for ensuring an interconnection to the neck and lumbar 3D-CRT fields. In a last step,

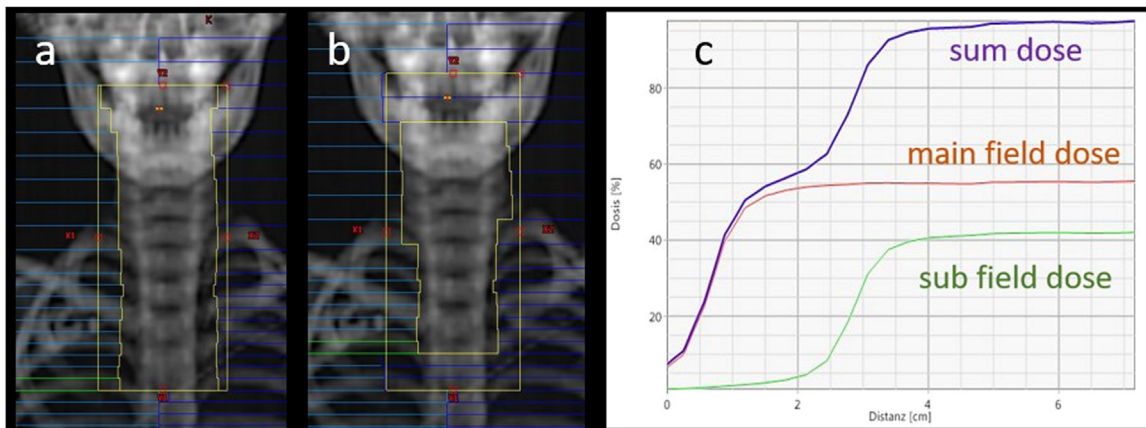


Fig. 3. MLC leaf positions of the 3D-CRT neck subsection. In (A) the leaf positions of the main field are shown. In (B) the leaf positions of the MLC subfield are shown. Both fields were further merged into an overall field-in-field. In (C) the sum dose of the merged field at the field boundary is shown, as well as the corresponding doses of the main and the sub fields. (Color version of figure is available online.)

Table 1A

PTV dose acceptance criteria, (95% of the prescribed dose = 33.4 Gy)

PTV dose acceptance	
D_{max}	≤ 107%
D_{mean}	= 100%
D_{95}	> 98%

the spine PTV dose coverage was optimized by dose weighting the single fields.

For the brain section, the above-described VMAT technique (3 VMAT arcs at IC1) is applied and completes the HybTP configuration.

HybTP field connection management

A stable field connection between 3D-CRT and VMAT fields succeeds if the dose at the field boundaries of the 3D-CRT fields does not fall off steeply, but decreases gradually with a step function. Such a dose drop can be modeled using the field-in-field function of the TPS. A subfield with cranially and caudally closed MLC is integrated into the main 3D-CRT field. The subfield must be weighted in such a way that a step-shaped dose distribution results, as shown exemplarily for the cranial field connection in Figs. 3A and B.

HT planning

HT treatment plan was planned with a single isocenter (IC) for to be treated at a Tomo HDA™ (Version 2.1.2, Accuray Incorporated, Sunnyvale, CA). For this purpose, the data set was transferred to Accuray® Planning Station (Version 5.1.1.6, Accuray Incorporated, Sunnyvale, CA). The completed treatment plan was finally exported into TPS Eclipse in order to be able to compare it with the other techniques.

Plan acceptance criteria

In Table 1A and B the defined plan acceptance criteria for PTV and OARs are shown.

Moreover, the calculated plans were compared based on matching the dose criteria, the conformity index (CI) and homogeneity index (HI).

The conformity index is calculated as $CI = \frac{TV_{RI} \times TV_{RI}}{TV \times V_{RI}}$

Table 1B

Dose acceptance criteria for OARs

Organ	Dose acceptance	
Lenses	D_{max}	< 10 Gy
Lung	D_{mean}	< 7 Gy
Kidneys	D_{mean}	< 15 Gy
Heart	D_{mean}	< 26 Gy
Heart	V_{25}	< 10%

Where TV means Target Volume, V_{RI} Volume of the Reference Isodose and TV_{RI} the Target Volume which is covered by the Reference Isodose.⁴⁰

The homogeneity index is calculated as $HI = \frac{D_{PTV}(2\%) - D_{PTV}(98\%)}{D_{PTV}(50\%)}$

Where $D_{PTV}(x\%)$ means the dose which is received by $x\%$ of the PTV volume.

Furthermore, the organ doses are compared with each other, as well as the Volume of body receiving a low dose of 5 Gy ($V_5=x\%$).

Evaluation plan robustness

As CSI using conventional LINACS are treatments with multiple isocenters an evaluation of robustness against positioning uncertainties and potential intrafractional motion, especially at the field junctions, is essential.

To simulate a cranio-caudal positioning inaccuracy, HybTP plans were calculated in which the table position was shifted caudally and cranially. A caudal table shift simulates a field shift out of each other (out), a cranial table shift simulates a field shift into each other (in). The resulting minimum and maximum doses respectively at the field interconnections were recorded and compared to table shifts of VMAT and 3D-CRT plans. Similarly, the resulting CI and HI values were calculated after performing the table shifts.

Results

PTV dose coverage

All planning techniques match the plan acceptance criteria, namely that the maximum dose does not exceed 107% of the prescribed dose while the mean dose equals 100%, and that 98% of the PTV volume is covered by at least 95% (=33.4 Gy) of the prescribed dose.

The highest conformity index was achieved when using HT. VMAT and IMRT were similar, whereas 3D-CRT and HybTP achieve lower conformity indices.

HT and IMRT plans resulted in highly homogenous dose distributions. The homogeneity indices of 3D-CRT, HybTP and VMAT were similar but lower than the indices of HT and IMRT.

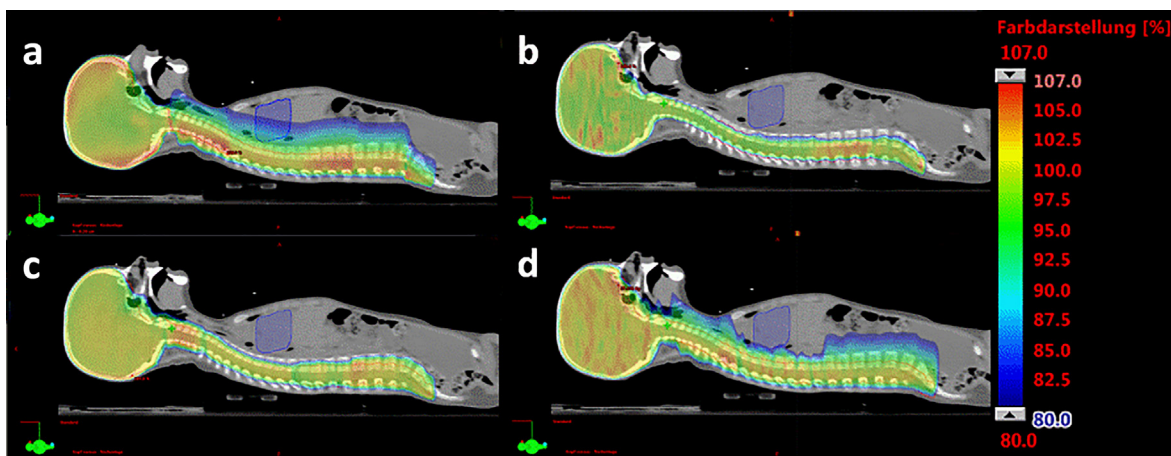


Fig. 4. Sagittal view dose distributions different techniques, heart structure in blue, dose shown in color wash scaled from 80 to 107%. (A) 3D-CRT, 80% isodose through heart. (B) VMAT, 80% no isodose through the heart. (C) IMRT, 80% no isodose through the heart. (D) HybTP, heart protection by VMAT rotation at heart region, in contrast to 3D-CRT no 80% isodose through the heart. (Color version of figure is available online.)

Table 2

Dose received by 98% of PTV Volume (D_{98}), conformity index (CI), homogeneity index (HI) and % of Volume receiving a low dose of 5Gy ($V_5 = x\%$) for the different planning techniques

Index	3D-CRT	VMAT	HybTP	IMRT	HT
D_{98}	98.2%	98.4%	99.1%	99.4%	98.7%
CI	0.83	0.96	0.86	0.91	0.98
HI	0.13	0.14	0.15	0.07	0.07
V_5	40%	73%	43%	62%	55%

The lowest value for the V_5 was achieved with 3D-CRT followed by HybTP. VMAT, as a rotation method, resulted in the highest low-dose exposure. The achieved values for the different planning techniques are shown in Table 2.

Table 2 Dose received by 98% of PTV Volume (D_{98}), CI, HI and % of Volume receiving a low dose of 5Gy ($V_5 = x\%$) for the different planning techniques.

Doses at OARs

Table 3 below shows the maximum doses to the eye lenses, the mean doses to the other OARs, and the Volume of heart receiving a dose ≥ 25 Gy for the different planning techniques.

All defined dose acceptance criteria were met when applying HT. The right and left lenses received $D_{max} = 4.9$ Gy, the right lung $D_{mean} = 6.9$ Gy and the left lung $D_{mean} = 6.3$ Gy. The mean doses of the kidneys (right 3.7 Gy/left 3.9 Gy) and the mean dose of the heart (7.5 Gy) were below the defined dose limits; the V_{25} of the heart equals to 0%.

When applying 3D-CRT, the maximum doses were 32.3 Gy in the left and 33.1 Gy in the right lens respectively. These doses were higher than acceptable according to the defined acceptance criteria ($D_{max} < 10$ Gy). In contrast, sparing of kidneys (right 4.5 Gy/left 4.6 Gy) and lungs (right 5.4 Gy/left 6.4 Gy) was realized appropriately. For the heart a mean dose of $D_{mean} = 22.1$ Gy was achieved, which is below the required $D_{mean} < 26$ Gy. However, it was not possible to meet the acceptance criteria $V_{25} < 10\%$. The proportion of the heart volume receiving > 25 Gy was 43.9%.

Also, IMRT planning did not lead to a sufficient sparing of the eye lenses. Both lenses (right 13.1/left 12.2 Gy) receive more than the acceptable $D_{max} < 10$ Gy. Also the dose acceptance criteria for the lung $D_{mean} < 7$ Gy were not met (right 11.1 Gy/left 11.2 Gy). However, the dose acceptance criteria for the kidneys $D_{mean} < 15$ Gy were met (right $D_{mean} = 7.5$ Gy/left $D_{mean} = 6.1$ Gy). The mean dose for the heart was 8.9 Gy meeting the requirement of $D_{mean} < 26$ Gy, the volume of the heart V_{25} receiving more than 25 Gy equals to 0%.

VMAT planning realized a sufficient sparing of the lenses (right 9.4 Gy/left 8.8 Gy), kidneys (right 9.8/left 10.3 Gy) and heart (9.1 Gy/ $V_{25} = 0\%$). But the $D_{mean} < 7$ Gy for the lungs was not met (left 10.2 Gy/right 10.4 Gy).

HybTP achieved all required dose acceptance criteria. The maximum doses to the lenses (right 9.7 Gy/left 9.5 Gy) were below 10 Gy, the mean doses to the kidneys (right 4.5 Gy/left 4.6 Gy) below 15 Gy, the mean doses to the lungs (right 6.9 Gy/left 6.6 Gy) below 7 Gy, and the mean dose to the heart (16.9 Gy) below 26 Gy. The V_{25} equals to 9.8% and hence less than 10%.

Figure 4 demonstrates the dose distributions of the different techniques. Applying 3D-CRT (Fig. 4A) leads to an 80% isodose through the heart as a consequence of the dose dorsal field configuration. VMAT (Fig. 4B) and IMRT (Fig. 4C) keep the

80% isodose close to the spine PTV, resulting in the reduction of dose to the heart. Figure 4D demonstrates the dose distribution of HybTP. Compared to 3D-CRT the 80% isodose shows the impact of the cardiac integrated VMAT section.

Plan robustness

In Table 4 the minimum doses for caudal table shift (out) and the maximum doses for cranial table shift (in) from 1 mm and 2 mm shown. In the not shifted regular plan HybTP has a doses minimum of 98.1% at the field interconnection that falls down to 90.4% when a 1 mm out shift is applied. VMAT falls up from 97.8% to 91.7% and 3D-CRT from 97.2% to 86.7%. A 2 mm out shift leads to minimum dose of 82.9% for HybTP, 83.7% for VMAT and 73.4% for 3D-CRT. A 1 mm in shift leads to a dose maximum for HybTP of 110.7%, for VMAT 107.6%, and for 3D-CRT 117.8%. A 2 mm in shift leads to 121.4% for HybTP, 115.5% for VMAT, and 129.0% for 3D-CRT. For all regular plans, the maximum dose at the field interconnection was approx. 105% (Table 4).

In Tables 5 and 6 the values for CI and HI are listed, after performing OUT and IN table shifts. The differences to CI and HI without table shift (Tables 2 and 3) are shown in parenthesis. It can be seen that CI assumes lower values for all techniques after performing a table shift. 3D-CRT and HybTP reacts in a range of $\Delta CI = 0.05$ -0.06 and VMAT and IMRT in a range of $\Delta CI = 0.09$ -0.13. The HI stays almost unaffected by table shift varying in a range of $\Delta HI = 0.01$ -0.02 over all techniques.

Discussion

The hybrid treatment planning (HybTP) for CSI was developed with the motivation to meet the results of the HT technique with a Varian DHX CLINAC as close as possible. For CSI on a conventional LINAC currently 2 fundamentally different concepts exist. Static forward planned 3D-CRT and inverse planned modulated techniques IMRT and VMAT.⁴⁴ Both concepts lead to particular results that are not achievable by the other concept, but none of them can match the results of the HT. If it were possible to merge the both concepts into a hybrid technique that combines the respective advantages of the concepts and reduces the disadvantages, a third concept would emerge, the HybTP, opening new possibilities for approaching to HT. The results obtained with HybTP were discussed above in contrast to those of 3D-CRT, IMRT, VMAT and HT in terms of CI and HI, dose coverage at the cribriform plate, low body dose (V_5), and doses at OARs.

The lowest conformal index CI was obtained for 3D-CRT planning (CI=0.83). This is due to the low conformal dose coverage along the spinal PTV. Due to the single dorsal static field, this cannot be achieved to the quality as it is the case for VMAT (CI=0.96) and HT (CI=0.98). The HybTP also contains dorsal static fields in the spinal area, where the dose coverage of the PTV does not reach the quality of VMAT and IMRT. However, the VMAT field does not cover the entire length of the spinal PTV, as is the case with the

Table 3
Achieved mean and maximum doses at OARs and V25 at the heart

OARs	D _{mean}		IMRT		VMAT		HybTP		HT	
	3D-CRT		[Gy]	[%]	[Gy]	[%]	[Gy]	[%]	[Gy]	[%]
	[Gy]	[%]								
Left lung	6.4	18.18	11.2	30.9	10.2	28.9	6.6	18.7	6.3	17.9
Right lung	5.4	15.34	11.1	26.5	10.4	29.5	6.9	19.6	6.9	19.8
Left kidney	4.4	12.5	6.1	17.2	10.3	29.2	4.6	13.0	3.9	11.3
Right kidney	4.4	12.5	7.5	21.4	9.8	27.8	4.5	12.7	3.7	10.6
Heart	22.1	59.6	8.9	25.4	9.1	25.8	16.9	48.0	7.5	21.4
OARs	D _{max}		IMRT		VMAT		HybTP		HT	
	3D-CRT		[Gy]	[%]	[Gy]	[%]	[Gy]	[%]	[Gy]	[%]
	[Gy]	[%]								
Left lense	32.3	(91.76)	12.2	(34.8)	8.8	(25.0)	9.5	(24.4)	4.9	(14.2)
Right lense	33.1	(94.03)	13.1	(37.3)	9.4	(26.7)	9.7	(23.6)	4.9	(14.0)
Doses heart										
		3D-CRT		IMRT		VMAT		HybTP		HT
V ₂₅ [%]		43.9		0.0		0.0		9.8		0
D _{mean} [Gy]		22.1		8.9		9.1		16.9		7.5

Table 4
Minimum and maximum doses [%] at the field interconnection after table shift. The regular doses (Reg.) means the minimum, respectively maximum, dose for the not shifted plan

	Reg.	Caudal shift (out)		Reg.	Cranial shift (in) max	
		min Doses [%]			Doses [%]	
		1 mm	2 mm		1 mm	2 mm
HybTP	98.1	90.4	82.9	105.2	110.7	121.4
VMAT	97.8	91.7	83.7	105.0	107.6	115.5
3D-CRT	97.2	86.7	73.4	105.7	117.8	129.0

Table 5
CI values after performing of 1 mm and 2 mm table shift IN/OUT. The differences to the values without table shifts are shown in parenthesis

CI	3D-CRT	VMAT	HybTP	IMRT
1 mm OUT	0.78 (-0.05)	0.83 (-0.13)	0.81 (-0.05)	0.81 (-0.10)
2 mm OUT	0.78 (-0.05)	0.82 (-0.14)	0.81 (-0.05)	0.82 (-0.09)
1 mm IN	0.77 (-0.06)	0.83 (-0.13)	0.84 (-0.02)	0.82 (-0.09)
2 mm IN	0.77 (-0.06)	0.82 (-0.14)	0.81 (-0.05)	0.79 (-1.12)

Table 6
HI values after performing of 1 mm and 2 mm table shift IN/OUT. The differences to the values without table shifts are shown in parenthesis

HI	3D-CRT	VMAT	HybTP	IMRT
1 mm OUT	0.14 (+0.01)	0.14 (+0.0)	0.15 (+0.0)	0.08 (+0.01)
2 mm OUT	0.15 (+0.02)	0.15 (+0.01)	0.16 (+0.01)	0.09 (+0.02)
1 mm IN	0.14 (+0.01)	0.14 (+0.0)	0.15 (+0.0)	0.08 (+0.01)
2 mm IN	0.14 (+0.01)	0.15 (+0.01)	0.17 (+0.02)	0.07 (0.0)

3D-CRT technique. However, in addition, as with the pure VMAT technique, there is a high degree of conformity in the superior region. These facts result in a CI for HybTP of 0.86, which is slightly better than the pure 3D-CRT technique, but overall worse than VMAT. IMRT achieves good conformation in the spinal region but not in the skull, resulting in a CI of 0.91. This is consistent with a plan comparison study from Herdian et al.⁵³ in which they stated that IMRT and HT techniques are able to achieve better conformities than 3DCRT. Srivastava et al. came to the same conclusion in a similar comparative study.⁵⁶ The homogeneity indices of 3D-CRT (HI=0.13), VMAT (HI=0.14) and HybTP (HI=0.15) are comparatively close together. The HI for IMRT and HT are both 0.07. In the case of an ideal dose homogeneity the HI would take the value of

0. Even though the highest HI was determined for HybTP, all values are around 0 and thus differ only marginally in terms of dose homogeneity.

Frequently, the argument for using the 3D-CRT technique is that highly conformal techniques such as VMAT increase the risk of developing a radiation-induced second tumor due to the higher low-dose volume.^{23,29,50} 3D-CRT has the smallest body low-dose volume V₅ of 40%, directly followed by HybTP with V₅=43%. For the other techniques, the values are higher (HT 55%, IMRT 62%, VMAT 72%). Lang et al. used a hybrid treatment technique consisting of VMAT and 3D field-in-field segments for irradiation of a chest wall and regional lymph nodes after mastectomy. They too found that hybrid plans were more effective in avoiding the spread of low doses to healthy tissue.⁵⁶

The fact that the V₅ of 3D-CRT and HybTP is very similar can be explained by the composite field technique of HybTP. The skull region has on the low dose exposure marginal relevance, since it consists mainly of PTV and less normal tissue. HT, IMRT and VMAT cause higher low-dose exposure than 3D-CRT. Since HybTP is composed of 3D-CRT fields and only in the cardiac region a VMAT technique is used, the low dose range is lowered accordingly.

With HybTP the eye lenses received doses of 9.7 Gy in the right and 9.5 Gy in the left lens. Emami et al.⁴⁸ showed that a cataract can develop (TD 5/5) after low-dose exposure and suggested a dose constraint of 10 Gy when applying conventional fractionation. This constraint is also successfully achieved with HT (left 4.9 Gy/right 4.9 Gy) and VMAT (left 8.8 Gy/right 9.4 Gy). With IMRT a dose coverage of the cribriform plate could be realized, but it was not possible to achieve a lens protection <10 Gy.

The lens dose of the HybTP is higher than that of the VMAT, although both techniques include the same field configuration. With HybTP, however, scattering of the adjacent spinal 3D-CRT field is added. Applying 3D-CRT the eye lenses received a dose >30 Gy which immensely increases the risk of forming a cataract. The actual benefit of using the HybTP at the skull instead of the 3D-CRT method lies in the dose coverage of the cribriform plate. In a survey including 40 medulloblastoma patients, Jereb et al.¹³ found 15% of all recurrences occurred in this region, if it was not adequately treated. According to Goswami et al.⁵⁴, for medulloblastoma patients, approximately 15-20% of recurrences occurs at the cribriform plate due to excessive shielding to protect ocular structures.

HybTP achieved a D_{mean} = 16.9 Gy of the heart, which is below the D_{mean} = 22.1 Gy of 3D-CRT. The heart doses of IMRT

($D_{mean} = 8.9$ Gy) and VMAT ($D_{mean} = 9.1$ Gy) are low and close to HT ($D_{mean} = 7.5$ Gy). The 3D-CRT D_{mean} is still within the dose acceptance criteria of <25 Gy, but the volume of the heart which receives a dose >25 Gy is 43.9% and does not meet the defined acceptance criteria of $<10\%$. According to the Quantec table, the probability of long-term cardiac mortality is higher than 1% for $V_{25} > 10\%$.⁴⁶ By applying the HybTP, HT, VMAT, and IMRT the $V_{25heart}$ can be reduced to almost 0. Ratoso et al.⁴⁷ explored in 2019 literature related to cardiotoxicity following mediastinal irradiation. They stated that studies uniformly show a linear radiation dose-response relationship between mean absorbed dose to the heart and the risk of dying as a result of cardiac disease. Therefore, dose to the heart should be an important aspect when evaluating CSI plans and is clearly the major drawback of the dorsal static field technique in 3D-CRT.

The mean doses in the lungs differ only marginally between 3D-CRT (right: 5.4 Gy/left: 6.4 Gy) and HybTP (right: 6.6 Gy/left: 6.9 Gy), which has been a major goal when developing HybTP. This can be explained by 2 facts. First, the leaves of the MLC in the superior 3D field segment still cover one third of the lung volume, which contributes to lung sparing. Second, the lung dose can be controlled within the possible range via the VMAT optimization module in the TPS. In comparison, the pure VMAT technique is not able to save the lungs in that range (lung right: 10.4 Gy/lung left: 10.2 Gy), neither is IMRT (lung right: 11.1 Gy/lung left: 11.2 Gy). With HT the lungs receive right 6.9 Gy and left 6.3 Gy. The dose constraint for the lungs corresponds to QUANTEC,⁴⁶ specifying the risk of symptomatic pneumonitis to be 5% if D_{mean} is 7 Gy.

The acceptance criteria for the kidney $D_{mean} < 15$ Gy is met by all techniques with a risk of a clinically relevant renal dysfunction below 5%.⁴⁶ The lowest values for D_{mean} were achieved with 3D-CRT (left: 4.4 Gy / right: 4.4 Gy) and HybTP (left: 4.6 Gy/right: 4.5 Gy). These values are close together, which was similar to the lung a primary objective in developing the HybTP.

In summary, only HybTP and HT meet all dose acceptance criteria of the OARs defined in Table 1. VMAT fails to meet the criteria for lungs, IMRT for lungs and eye lenses and 3D-CRT for heart and eye lenses.

The results presented here are consistent with results of the existing literature. Sharma et al. performed a comparative study between 3D-CRT, IMRT and HT. When IMRT and HT were used, the D_{mean} for lungs and kidneys increased compared to 3D-CRT. Although the increase is not of the same range as in our study, this qualitatively confirms our thesis of dose minimization of lungs and kidneys by using 3D-CRT.⁴ Regarding eye sparing, they come up with comparable high dose values for 3D-CRT and IMRT ($D_{mean,eyes} > 35$ Gy). Only with HT they were able to keep the doses below 8 Gy. Pollul et al. compared a short partial-arc VMAT technique with 3D-CRT planning in a study including 24 patients. In sum they were VMAT planned able to achieve a $D_{mean,heart} = 6.6$ Gy compared to $D_{mean} = 16.0$ Gy with 3D-CRT. Regarding mean doses for kidneys and lungs, they also could not achieve VMAT planned lower values than with 3D-CRT (VMAT $D_{mean,lung} = 7.5$ Gy, 3D-CRT $D_{mean,lung} = 4.2$ Gy/VMAT $D_{mean,kidney} = 5.3$ Gy, 3D-CRT $D_{mean,kidney} = 2.6$ Gy).⁵² Pichandi et al.²⁰ report similar results. In the study of de Saint-Hubert lungs and kidneys were more effectively spared with 3D-CRT than with IMRT and HT.²⁵ Seravalli et al. performed a study across 15 European centers, comparing 3D-CRT, IMRT, VMAT, HT, and Proton plans calculated with 1 identical CT-dataset, similar to our study. They reported qualitatively about the same relationships: lowest values for lungs and kidneys with 3D-CRT, low $D_{mean,heart}$ by applying IMRT, VMAT, and HT. In contrast to our results is a $D_{lens,median} < 6$ Gy for 3D-CRT, which also cannot be surpassed by any other techniques.³⁶ Other studies are able to achieve $D_{mean,lung} < 7$ Gy with dose prescriptions analog to our scheme even with VMAT and IMRT.^{4,28} This is well below our

results. It would be interesting to compare HybTP with IMRT and VMAT plans from other radiotherapy facilities, with defined starting assumptions.

When interpreting our results, one has to be aware that the study includes only a single patient. Therefore, it must be considered as a proposal for an alternative planning strategy. The principle approach, i.e., selectively merging of field segments of prioritized techniques, remains the same regardless of patient anatomy. Although the HybTP was developed for a CLINAC 2100 DHX, this technique can in principle also be adapted for other LINAC types.

With HybTP, an additional possibility to optimize PTV dose coverage-low dose exposure-saving OARs exists. For example, departments facing the challenge of treating young patients with pre-existing lung or kidney disease may now have a planning option if patients could tolerate a higher coronary dose by reduced low-dose exposure. Similarly, simultaneous sparing of the hippocampus and hypothalamic-pituitary axis, as mentioned by Zheng et al.³¹ would be possible.

The treatment of a CSA on a LINAC needs special attention regarding positioning inaccuracies and the resulting inhomogeneities at the field junctions. To increase plan robustness, the field junctions of 3D-CRT plans must be shifted after a certain number of fractions.^{18,19} VMAT plans can be created with overlapping fields, with the goal achieving a uniform dose across the transition to minimize robustness to field placement errors.³⁰ A similar principle was to be applied to HybTP. The challenge was to combine 3D-CRT fields with generally steep dose falloffs, overlapping with flat fallen doses from VMAT fields. This was realized by using the field-in-field function of the TPS when structuring the 3D-CRT fields. By overlaying 3D-CRT fields of different field lengths, a dose falloff similar to a step function could be modeled, approximated to the typical flatter falling dose profiles of VMAT fields. As a result of the intersecting field dose components, HybTP plans are not as sensitive to positioning inaccuracies or intrafraction movement as 3D-CRT plans. Further effort should be taken to make the HybTP as robust as the VMAT is. Whether field feathering for HybTP is necessary or not should be discussed from case to case after field displacement analysis and clinically internal evaluation of the estimated maximal positioning inaccuracies. A plan robustness analysis with respect to CI or HI after a positioning inaccuracy of up to 2 mm showed that all planning variants react only marginally to such a scenario (VMAT/IMRT $\Delta CI = 0.09-0.13$ /3D-CRT/HybTP $\Delta CI = 0.05-0.06$ and ΔHI all techniques = 0.01-0.02). In addition, it is important to bear in mind that a displacement of 2 mm, as assumed in our studies for high-precision radiotherapy with vacuum mattress positioning, is a relatively high order of magnitude. In principle, such a displacement should already be excluded by a high degree of quality assurance.

As with any comparative planning study, this work is limited by the planning beam geometries and the optimization parameters used to generate the dose distribution. While the authors recognize that alternate IMRT beam arrangements, additional full or partial VMAT arcs, or blocking structures might yield lower doses to specific organs at risk, this limitation does not subtract from the utility of the HybTP solution presented here.

Conclusion

For radiotherapy facilities equipped with conventional LINACS, HybTP offers a new planning strategy for irradiating CSA with results particularly comparable to those of HT.

A dose sparing of the eye lenses by simultaneous dose coverage of the lamina cribrosa is possible in a comparable range to VMAT. Compared to 3D-CRT cardiotoxicity is significantly reduced. Lungs and kidneys are spared as with HT to a maximum level minimizing

the risk of symptomatic pneumonitis and renal dysfunction. Compared to IMRT, VMAT and HT, the low-dose exposure of the body volume is reduced.

Dose homogeneity and conformity are better than with a 3D-CRT treatment. Plan robustness against positioning errors is increased compared to 3D-CRT.

For all planning techniques a positioning inaccuracy from 2 mm has only a marginal effect on CI and HI.

Thus, HybTP offers the opportunity to create highly individualized treatment plans customized to specific patient needs.

Conflict of Interest

The authors declare no conflicts of interest.

Funding

This research did not receive any specific grant from funding agencies in the public, commercial, or not-for-profit sectors.

References

- Cox, M.C.; Kusters, J.M.; Gidding, C.E.; et al. Acute toxicity profile of craniospinal irradiation with intensity-modulated radiation therapy in children with medulloblastoma: A prospective analysis. *Radiat. Oncol.* **10**(1):1–9; 2015 PMID: 26597178; PMCID: PMC4657242. doi:10.1186/s13014-015-0547-9.
- Ostrom, Q.T.; Gittleman, H.; Farah, P.; et al. CBRUS statistical report: Primary brain and central nervous system tumors diagnosed in the United States in 2006–2010. *Neuro. Oncol.* **15**:646–7; 2013 Erratum in: *Neuro Oncol.* 2014 May;16(5):760. PMID: 24137015; PMCID: PMC3798196. doi:10.1093/neuonc/nwt151.
- Skowrońska-Gardas, A.; Chojnacka, M.; Morawska-Kaczyńska, M.; et al. Patterns of failure in children with medulloblastoma treated with 3D conformal radiotherapy. *Radiother. Oncol.* **84**(1):26–33; 2007 PMID: 17560676. doi:10.1016/j.radonc.2007.05.018.
- Sharma, D.S.; Gupta, T.; Jalali, R.; et al. High-precision radiotherapy for craniospinal irradiation: Evaluation of three-dimensional conformal radiotherapy, intensity-modulated radiation therapy and helical TomoTherapy. *Br. J. Radiol.* **82**:1000–9; 2009 Epub 2009 Jul 6. PMID: 19581313; PMCID: PMC3473394. doi:10.1259/bjir/13776022.
- Kiltie, A.E.; Lashford, L.S.; Gattamaneni, H.R. Survival and late effects in medulloblastoma patients treated with craniospinal irradiation under three years old. *Med. Pediatr. Oncol.* **28**(5):348–54; 1997 PMID: 9121399. doi:10.1002/(sici)1096-911x(199705)28:5<348:aid-mpo4>3.0.co;2-h.
- Hatten, M.E.; Roussel, M.F. Development and cancer of the cerebellum. *Trends Neurosci.* **34**(3):134–42; 2011 PMID: 21315459; PMCID: PMC3051031. doi:10.1016/j.tins.2011.01.002.
- Mani, K.R.; Sapru, S.; Maria Das, K.J.; et al. A supine cranio-spinal irradiation technique using moving field junctions. *Polish J. Med. Phys. Engin.* **22**(4):79–83; 2016. doi:10.1515/pjmpe-2016-0014.
- Northcott, P.A.; Robinson, G.W.; Kratz, C.P.; et al. Medulloblastoma. *Nat. Rev. Dis. Primers.* **5**(1):11; 2019 PMID: 30765705. doi:10.1038/s41572-019-0063-6.
- Millard, N.E.; De Braganca, K.C. Medulloblastom. *J. Kind. Neurol.* **31**(12):1341–53; 2016 Epub 2015 Sep 2. Erratum in: *J Child Neurol.* 2016 Sep 15; PMID: 26336203; PMCID: PMC4995146. doi:10.1177/0883073815600866.
- Mahapatra, S.; Amsbaugh, M.J. Medulloblastoma. *StatPearls [Internet], Treasure Island FL: StatPearls Publishing; 2022. PMID: 28613723.*
- Jefferies, S.; Rajan, B.; Ashley, S.; et al. Haematological toxicity of craniospinal irradiation. *Radiother. Oncol.* **48**(1):23–7; 1998 PMID: 9756168. doi:10.1016/s0167-8140(98)00024-3.
- Bandurska-Luque, A.; Piotrowski, T.; Skrobala, A.; et al. Prospective study on dosimetric comparison of helical tomotherapy and 3DCRT for craniospinal irradiation - A single institution experience. *Rep. Pract. Oncol. Radiother.* **20**(2):145–52; 2015 PMID: 25859405; PMCID: PMC4338290. doi:10.1016/j.rpor.2014.12.002.
- Jereb, B.; Krishnaswami, S.; Reid, A.; et al. Radiation for medulloblastoma adjusted to prevent recurrence to the cribriform plate region. *Cancer* **54**(3):602–4; 1984 PMID: 6733691. doi:10.1002/1097-0142(19840801)54:3<602:aid-cnrcr2820540336>3.0.co;2-y.
- Uozumi, A.; Yamaura, A.; Makino, H.; et al. A newly designed radiation port for medulloblastoma to prevent metastasis to the cribriform plate region. *Childs Nerv. Syst.* **6**(8):451–5; 1990 PMID: 2095305. doi:10.1007/BF00302092.
- Kochbati, L.; Ghorbel, I.; Chaari, N.; et al. Rechute frontale du médulloblastome: Causes et conséquences (à propos d'un cas). *Cancer/Radiothérapie.* **12**(Issue 8):860–2; 2008 ISSN 1278-3218.
- Gupta, M.; Ahmad, M. Pediatric medulloblastoma: A radiation oncologist perspective. *Brain and Spinal Tumors - Primary and Secondary.* Morgan L.R., Sarica F.B., editors. *IntechOpen*; 2019. doi:10.5772/intechopen.84344.
- Gripp, S.; Kamberg, J.; Wittkamp, M.; et al. Coverage of anterior fossa in whole-brain irradiation. *Int. J. Radiat. Oncol. Biol. Phys.* **59**(2):515–20; 2004 PMID: 15145171. doi:10.1016/j.ijrobp.2003.10.030.
- Rades, D.; Holtzhauer, R.; Baumann, R.; et al. Craniospinal axis irradiation in children. Treatment in supine position including field verification as a prerequisite for anesthesia without intubation. *Strahlenther. Onkol.* **175**(8):409–12; 1999 PMID: 10481774. doi:10.1007/s000660050030.
- Parker, W.A.; Freeman, C.R. A simple technique for craniospinal radiotherapy in the supine position. *Radiother. Oncol.* **78**(2):217–22; 2006 Epub 2005 Dec 5. PMID: 16330119. doi:10.1016/j.radonc.2005.11.009.
- Pichandi, A.; Ganesh, K.M.; Jerrin, A.; et al. Cranio spinal irradiation of medulloblastoma using high precision techniques - a dosimetric comparison. *Technol. Cancer Res. Treat.* **14**(4):491–6; 2015 PMID: 26269611. doi:10.1177/1533034614500421.
- Bernier, V.; Klein, O. Late effects of craniospinal irradiation for medulloblastomas in paediatric patients. *Neurochirurgie.* **67**(1):83–6; 2021 Epub 2018 Aug 24. PMID: 30149928. doi:10.1016/j.neuchi.2018.01.006.
- Wang, Z.; Jiang, W.; Feng, Y.; et al. A simple approach of three-isocenter IMRT planning for craniospinal irradiation. *Radiat. Oncol.* **8**:217; 2013 PMID: 24044521; PMCID: PMC3851431. doi:10.1186/1748-717X-8-217.
- Brodin, N.P.; Munck Af Rosenschöld, P.; Aznar, M.C.; et al. Radiobiological risk estimates of adverse events and secondary cancer for proton and photon radiation therapy of pediatric medulloblastoma. *Acta. Oncol.* **50**(6):806–16; 2011 PMID: 21767178. doi:10.3109/0284186X.2011.582514.
- Lee, Y.K.; Brooks, C.J.; Bedford, J.L.; et al. Development and evaluation of multiple isocentric volumetric modulated arc therapy technique for craniospinal axis radiotherapy planning. *Int. J. Radiat. Oncol. Biol. Phys.* **82**(2):1006–12; 2012 Epub 2011 Feb 23. PMID: 21345612. doi:10.1016/j.ijrobp.2010.12.033.
- De Saint-Hubert, M.; Verellen, D.; Poels, K.; et al. Out-of-field doses from pediatric craniospinal irradiations using 3D-CRT, IMRT, helical tomotherapy and electron-based therapy. *Phys. Med. Biol.* **62**(13):5293–311; 2017 Epub 2017 Apr 11. PMID: 28398210. doi:10.1088/1361-6560/aa6c9e.
- Tatcher, M.; Glicksman, A.S. Field matching considerations in craniospinal irradiation. *Int. J. Radiat. Oncol. Biol. Phys.* **17**(4):865–9; 1989 PMID: 2777678. doi:10.1016/0360-3016(89)90080-1.
- Wang, K.; Meng, H.; Chen, J.; et al. Plan quality and robustness in field junction region for craniospinal irradiation with VMAT. *Phys. Med.* **48**:21–6; 2018 Epub 2018 Mar 23. PMID: 29728225. doi:10.1016/j.ejmp.2018.03.007.
- Myers, P.; Stathakis, S.; Gutiérrez, A.; et al. Dosimetric comparison of craniospinal axis irradiation (CSI) treatments using helical tomotherapy, SmartarcTM, and 3D conventional radiation therapy. *Int. J. Med. Phys., Clin. Engin. Radiat. Oncol.* **2**(1):30–8; 2013. doi:10.4236/ijmpcero.2013.21005.
- Wong, K.K.; Ragab, O.; Tran, H.N.; et al. Acute toxicity of craniospinal irradiation with volumetric-modulated arc therapy in children with solid tumors. *Pediatr. Blood Cancer.* **65**(7):e27050; 2018 Epub 2018 Apr 6. PMID: 29630782. doi:10.1002/pbc.27050.
- McVicar, N. Improved volumetric modulated arc therapy field junctions using in silico base plans: Application to craniospinal irradiation. *J. Med. Imaging Radiat.* **3**(9):301–8; 2018 Epub 2018 Jun 18. PMID: 32074057. doi:10.1016/j.jmir.2018.05.005.
- Zheng, J.; Aljabab, S.; Lacasse, P.; et al. Functional cranio-spinal irradiation: A hippocampal and hypothalamic-pituitary axis sparing radiation technique using two IMRT modalities. *Med. Dosim.* **45**(2):190–6; 2020 SummerEpub 2019 Dec 13. PMID: 31843470. doi:10.1016/j.meddos.2019.10.005.
- Studenski, M.T.; Shen, X.; Yu, Y.; et al. Intensity-modulated radiation therapy and volumetric-modulated arc therapy for adult craniospinal irradiation—a comparison with traditional techniques. *Med. Dosim.* **38**(1):48–54; 2013 SpringEpub 2012 Aug 9. PMID: 22878118. doi:10.1016/j.meddos.2012.05.006.
- Sarkar, B.; Munshi, A.; Ganesh, T.; et al. Dosimetric comparison of short and full arc in spinal PTV in volumetric-modulated arc therapy-based craniospinal irradiation. *Med. Dosim.* **45**(1):1–6; 2020 SpringEpub 2019 Apr 15. PMID: 30995966. doi:10.1016/j.meddos.2019.03.003.
- Li, Q.; Gu, W.; Mu, J.; et al. Collimator rotation in volumetric modulated arc therapy for craniospinal irradiation and the dose distribution in the beam junction region. *Radiat. Oncol.* **10**:235; 2015. doi:10.1186/s13014-015-0544-z.
- Thomadsen, B. Radiation oncology: A physicist's-eye view. *Med. Phys.* **36**:673; 2009. doi:10.1118/1.3068410.
- Seravalli, E.; Bosman, M.; Lassen-Ramshad, Y.; et al. Dosimetric comparison of five different techniques for craniospinal irradiation across 15 European centers: Analysis on behalf of the SIOP-E-BTG (radiotherapy working group). *Acta. Oncol.* **57**(9):1240–9; 2018 Epub 2018 Apr 26. PMID: 29698060. doi:10.1080/0284186X.2018.1465588.
- Schiopu, S.R.; Habl, G.; Häfner, M.; et al. Craniospinal irradiation using helical tomotherapy for central nervous system tumors. *J. Radiat Res.* **58**(2):238–46; 2017 PMID: 28096196; PMCID: PMC5439401. doi:10.1093/jrr/rw095.
- Welsh, J.S.; Patel, R.R.; Ritter, M.A.; et al. Helical tomotherapy: An innovative technology and approach to radiation therapy. *Technol. Cancer Res. Treat.* **1**(4):311–16; 2002 PMID: 12625791. doi:10.1177/153303460200100413.
- Coles, C.E.; Hooles, A.C.; Harden, S.V.; et al. Quantitative assessment of inter-clinician variability of target volume delineation for medulloblastoma: Quality assurance for the SIOP PNET 4 trial protocol. *Radiother. Oncol.* **69**(2):189–94; 2003 PMID: 14643957. doi:10.1016/j.radonc.2003.09.009.
- Van't Riet, A.; Mak, A.C.; Moerland, M.A.; et al. A conformation number to quantify the degree of conformality in brachytherapy and external beam irradiation: Application to the prostate. *Int. J. Radiat. Oncol. Biol. Phys.* **37**(3):731–6; 1997 PMID: 9112473. doi:10.1016/s0360-3016(96)00601-3.
- Lee, J.; Kim, E.; Kim, N.; et al. Pulmonary toxicity of craniospinal irradiation using helical tomotherapy. *Sci. Rep.* **12**(1):3221; 2022 PMID: 35217707; PMCID: PMC8881492. doi:10.1038/s41598-022-07224-1.

42. Holmes, J.A.; Chera, B.S.; Brenner, D.J.; et al. Estimating the excess lifetime risk of radiation induced secondary malignancy (SMN) in pediatric patients treated with craniospinal irradiation (CSI): Conventional radiation therapy versus helical intensity modulated radiation therapy. *Pract. Radiat. Oncol* **7**(1):35–41; 2017 Epub 2016 Jul 8. PMID: 27663930. doi:[10.1016/j.prro.2016.07.002](https://doi.org/10.1016/j.prro.2016.07.002).
43. Peñagaricano, J.; Moros, E.; Corry, P.; et al. Pediatric craniospinal axis irradiation with helical tomotherapy: Patient outcome and lack of acute pulmonary toxicity. *Int. J. Radiat. Oncol. Biol. Phys* **75**(4):1155–61; 2009 Epub 2009 May 19. PMID: 19467796. doi:[10.1016/j.ijrobp.2008.12.083](https://doi.org/10.1016/j.ijrobp.2008.12.083).
44. Oldham, M.; Neal, A.; Webb, S. A comparison of conventional 'forward planning' with inverse planning for 3D conformal radiotherapy of the prostate. *Radiother. Oncol* **35**(3):248–62; 1995 Erratum in: *Radiother. Oncol* 1995 Nov;37(2):171–2. PMID: 7480829. doi:[10.1016/0167-8140\(95\)01556-v](https://doi.org/10.1016/0167-8140(95)01556-v).
45. Fernandez-Vicioso, E., Ruiz-Cruces, R., & Faulkner, K. (2001). Tolerance of the different structures of the eye to therapeutic ionizing radiation (IAEA-CSP-7/CD). International Atomic Energy Agency (IAEA).
46. Marks, L.B.; Yorke, E.D.; Jackson, A.; et al. Use of normal tissue complication probability models in the clinic. *Int. J. Radiat. Oncol. Biol. Phys* **76**(3 Suppl):S10–19; 2010 PMID: 20171502; PMCID: PMC4041542. doi:[10.1016/j.ijrobp.2009.07.1754](https://doi.org/10.1016/j.ijrobp.2009.07.1754).
47. Ratosa, I.; Ivanetic Pantar, M. Cardiotoxicity of mediastinal radiotherapy. *Rep. Pract. Oncol. Radiother.* **24**(6):629–43; 2019 Epub 2019 Oct 30. PMID: 31719801; PMCID: PMC6838493. doi:[10.1016/j.rpor.2019.09.002](https://doi.org/10.1016/j.rpor.2019.09.002).
48. Emami, B.; Lyman, J.; Brown, A.; et al. Tolerance of normal tissue to therapeutic irradiation. *Int. J. Radiat. Oncol. Biol. Phys* **21**(1):109–22; 1991 PMID: 2032882. doi:[10.1016/0360-3016\(91\)90171-y](https://doi.org/10.1016/0360-3016(91)90171-y).
49. Williams, M.V. The cribriform plate: A sanctuary site for meningeal leukaemia. *Br. J. Radiol* **60**(713):469–75; 1987 PMID: 3472622. doi:[10.1259/0007-1285-60-713-469](https://doi.org/10.1259/0007-1285-60-713-469).
50. Followill, D.; Geis, P.; Boyer, A. Estimates of whole-body dose equivalent produced by beam intensity modulated conformal therapy. *Int. J. Radiat. Oncol. Biol. Phys* **38**(3):667–72; 1997 Erratum in: *Int J Radiat Oncol Biol Phys* 1997 Oct 1;39(3):783. PMID: 9231693. doi:[10.1016/s0360-3016\(97\)00012-6](https://doi.org/10.1016/s0360-3016(97)00012-6).
51. Sakthivel, V.; Ganesh, K.M.; McKenzie, C.; et al. Second malignant neoplasm risk after craniospinal irradiation in X-ray-based techniques compared to proton therapy. *Australas Phys. Eng. Sci. Med* **42**(1):201–9; 2019 Epub 2019 Feb 6. PMID: 30725439. doi:[10.1007/s13246-019-00731-y](https://doi.org/10.1007/s13246-019-00731-y).
52. Pollul, G.; Bostel, T.; Grossmann, S.; et al. Pediatric craniospinal irradiation with a short partial-arc VMAT technique for medulloblastoma tumors in dosimetric comparison. *Radiat. Oncol.* **15**:256; 2020. doi:[10.1186/s13014-020-01690-5](https://doi.org/10.1186/s13014-020-01690-5).
53. Herdian, F.; Lestari, A.A.S.A.; Jayalie, V.F.; et al. Analysis of dosimetric parameter on craniospinal irradiation with helical tomotherapy (HT), 3D conformal radiotherapy (3DCRT), and intensity modulated radiotherapy (IMRT). *Onkol. Radiotherap.* **14**(4):1–6; 2020.
54. Goswami, B.; Jain, R.; Yadav, S.; et al. Comparison of treatment planning parameters of different radiotherapy techniques for craniospinal irradiation. *Iran. J. Med. Phys.* **18**(3):164–70; 2021. doi:[10.22038/ijmp.2020.45574.1712](https://doi.org/10.22038/ijmp.2020.45574.1712).
55. Srivastava, R.; Saini, G.; Sharma, P.K.; et al. A technique to reduce low dose region for craniospinal irradiation (CSI) with RapidArc and its dosimetric comparison with 3D conformal technique (3DCRT). *J. Cancer Res. Ther* **11**(2):488–91; 2015 PMID: 26148626. doi:[10.4103/0973-1482.144556](https://doi.org/10.4103/0973-1482.144556).
56. Lang, K.; Loritz, B.; Schwartz, A.; et al. Dosimetric comparison between volumetric-modulated arc therapy and a hybrid volumetric-modulated arc therapy and segmented field-in-field technique for postmastectomy chest wall and regional lymph node irradiation. *Med. Dosim* **45**(2):121–7; 2020 SummerEpub 2019 Sep 27. PMID: 31570239. doi:[10.1016/j.meddos.2019.08.001](https://doi.org/10.1016/j.meddos.2019.08.001).